Nanoscale Res Lett (2006) 1:160–166
DOI 10.1007/s11671-006-9012-x

NANO EXPRESS

# Site-controlled quantum dots fabricated using an atomic-force microscope assisted technique

**H. Z. Song · T. Usuki · T. Ohshima · Y. Sakuma · M. Kawabe · Y. Okada · K. Takemoto · T. Miyazawa · S. Hirose · Y. Nakata · M. Takatsu · N. Yokoyama**

Published online: 3 August 2006


**Abstract** An atomic-force microscope assisted technique is developed to control the position and size of self-assembled semiconductor quantum dots (QDs). Presently, the site precision is as good as ± 1.5 nm and the size fluctuation is within ± 5% with the minimum controllable lateral diameter of 20 nm. With the ability of producing tightly packed and differently sized QDs, sophisticated QD arrays can be controllably fabricated for the application in quantum computing. The optical quality of such site-controlled QDs is found comparable to some conventionally self-assembled semiconductor QDs. The single dot photoluminescence of site-controlled InAs/InP QDs is studied in detail, presenting the prospect to utilize them in quantum communication as precisely controlled single photon emitters working at telecommunication bands.

**Keywords** Quantum dot · Site-Control · Atomic-force microscope · Local oxidation · Quantum computer · Quantum communication

H. Z. Song (✉) · T. Usuki · T. Ohshima · K. Takemoto · T. Miyazawa · S. Hirose · Y. Nakata · M. Takatsu · N. Yokoyama
Nanotechnology Research center, Fujitsu Lab. Ltd., Morinosato-Wakamiya 10-1, Atsugi, Kanagawa 243-0197, Japan
e-mail: song.hai-zhi@jp.fujitsu.com

Y. Sakuma · M. Kawabe
Nanomaterials Laboratory, National Institute for Materials Science (NIMS), Tsukuba, Ibaraki, Japan

Y. Okada
Institute of Applied Physics, University of Tsukuba, Tsukuba, Ibaraki 305-8773, Japan

## Introduction

In general, self-assembled semiconductor quantum dots (QDs) grown in Stranski–Krastanov (S–K) mode are randomly distributed both in position and size, which limits their possible applications [1]. Well ordered QD arrays are quite attractive in many applications such as optoelectronic devices. For example, two-dimensionally ordered and close-packed QDs may suppress the phonon scattering and enhance the optical non-linearity [2, 3]. In few cases, such an array can be self-organized by direct S–K growth.[4]. In recent years, self-assembled semiconductor QDs have been considered to be utilized in quantum information processing [5–8]. It requires well defined inter-dot coupling [9], putting demands on precise control of QD sites. Efforts have been devoted to define the positions of self-assembled QDs by means of, *e.g.*, scanning tunneling microscope lithography [10], strain modulation [11] and nanotemplate [12], but they seem difficult in constructing qubits mainly due to dot separation still being out of noticeable inter-dot coupling. We developed a technique assisted by atomic-force microscope (AFM), by which one can set QDs sufficiently close and prepare dot array sophisticated to fit the requirements of quantum information processing [13]. In this paper, we describe the characteristics of site-controlled semiconductor QDs fabricated using our AFM-assisted technique and their applications in quantum computation and quantum communication.

## Fabrication

Our AFM-assisted technique consists of three steps, briefly forming oxide dots, preparing holes and growing QDs.

The first stage is the fabrication of oxide dots, which is performed by AFM lithography at room temperature in a humid atmosphere. The substrate can be many semiconductors such as GaAs [13–15], InP [16] and Si [17] of any conduction type (n, p and intrinsic). As shown schematically in Fig. 1, when a negatively biased AFM tip approaches the flat surface of a semiconductor substrate, the electric field decomposes water molecules in the small region around the AFM tip into $H^+$ and $OH^-$. Then the $OH^-$ ions locally oxidize the surface. In the case of GaAs substrate, this reaction is as follows [18]

$$2GaAs + 12OH^- \rightarrow Ga_2O_3 + As_2O_3 + 6H_2O + 12e^- \quad (1)$$

Oxygen incorporation expands the volume and then contributes a part above the original surface, and then forms a nanoscaled oxide dot outstanding beyond the surface as shown in Fig. 1a. The oxidation rate depends on the electric field or current. Due to the pin-shape of a tip, the electric field/current decreases along the radial directions from the tip center. It thus gives rise to a lens-shaped oxide dot. The oxide dot size can be controlled by suitably tuning the applied voltage and reaction time.

The oxidized region is not limited above the original surface. Similar to the conventional oxidation of semiconductor surface, nearly half of the oxidized region lies below the original surface level, as can also be seen in Fig. 1a. If we remove the oxide, the space released from the oxide dot will give a hole. To remove the oxide dots, one can use chemical etching. The usually used solution is HCl : $H_2O$ = 1:20 ~ 1:100 at least for GaAs and InP. The etching time can be from 30 s to a few minutes. After etching, site-controlled holes are obtained, as shown schematically in Fig. 1b. Immediately, the hole-patterned substrate is rinsed in flowing de-ionized water for enough time so that the surface is of little residual solution. An alternative way to remove oxide dots is ultrasonic cleaning in water, whose mechanism may be that the structure of the oxide is so relaxed that the atomic bonding is weaker than in bulk semiconductor.

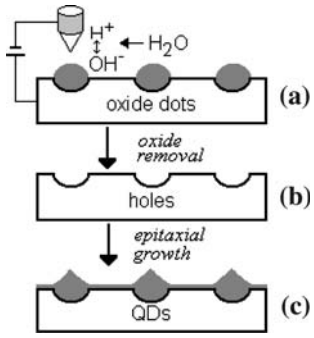


**Fig. 1** Process of AFM-assisted control of semiconductor QDs

As the final process, QDs are epitaxially grown by methods such as molecular beam epitaxy (MBE) and metalorganic chemical vapor deposition (MOCVD) on the hole-patterned surface. Before overgrowing, the thin oxide layer, which is formed in the short time of mounting the sample into the growth chamber, has to be cleaned away from the surface. It is unsuitable to carry out thermal cleaning because the hole pattern may be smeared out or even destroyed at temperature as high as 600 °C. We can use irradiation of atomic hydrogen at temperature below 550 °C for a few minutes. Hereafter, heteroepitaxy is performed to grow QDs at the same temperatures as normally used for QD growth in S–K mode. The coverage is limited below the point of transition from two to three dimensional growth modes, which is a fundamental factor in S–K growth of self-assembled QDs. With growth condition well controlled, QDs are formed on the sites of holes as shown in Fig. 1c. This site-selective growth of QDs may be understood by more strain-relaxation at the hole sites [15], although other explanations such as concentration of atomic steps [10] can not be completely excluded.

## Controlability

We shall now demonstrate how well the QDs can be controlled by our AFM-assisted technique. As an example, Fig. 2 shows the results of fabricating a square-latticed array with site-site distance of 50 nm on the surface of an $n^+$-GaAs (001) substrate ($2 \times 10^{18}$ $cm^{-2}$ Si-doped). Apart from the AFM images, line profiles, which were taken from somewhere in the AFM images along the centers of a chain of sites, are also given as a reference. The oxide dots seen in Fig. 2a are nearly of round shape in base and rather homogeneous in diameter, 32–36 nm. The line profile shows a reasonably small variation of the height of oxide dots, 1.2 –1.6 nm. The hole diameters seen in Fig. 2b, 32–36 nm, well follow that of the oxide dots. The line profile indicates the depth of the holes, 1.1–1.5 nm, which is similar to the height of the oxide dots as expected. The surface roughness looks a bit larger than that before etching due to the etching effect of native oxide on the flat area. However, this roughness does not influence the precision of hole pattern at all. Figure 2c shows the QDs array after MBE growth of $In_{0.4}Ga_{0.6}As$ at 490°C for

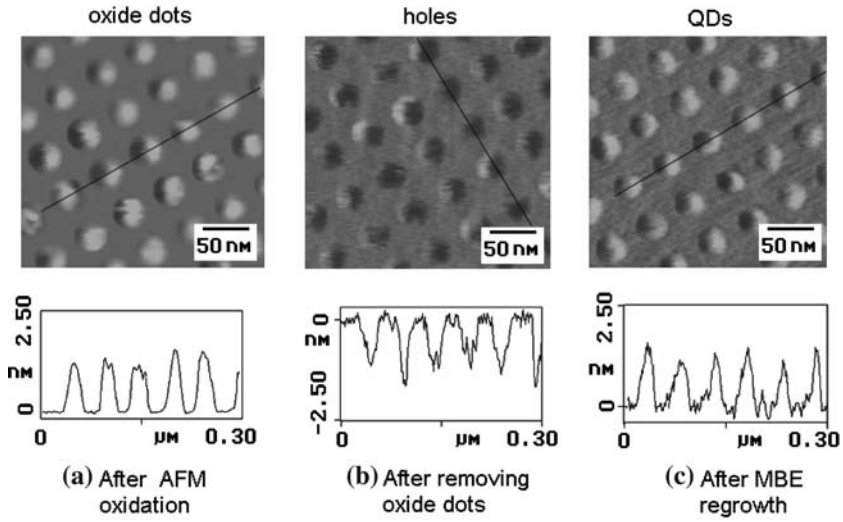


**Fig. 2** Top-view AFM images and line profiles of a square-latticed array after (**a**) AFM oxidation, (**b**) oxide dots removal by chemical etching and (**c**) 4.4 ML of $In_{0.4}Ga_{0.6}As$ regrowth by MBE. The lines in the images indicate where the profiles are taken

4.4 ML. The QDs are well organized into the expected square-latticed array. It implies that the QDs exactly locate on the sites of holes formed in (b). The diameters of QDs, 32 ~ 36 nm, are consistent with the oxide dots and holes. As a whole, the size fluctuation of about ± 5% is much better than usual S–K growth and comparable to very recently achieved homogeneity of S–K QDs [19]. The height and depth fluctuations, ~ 0.4 nm here, are reasonably small.

The precise QD control of our technique keeps working well until the inter-site distance gets down to less than 1.5 times of the hole diameter. In the upper half of Fig. 3, one line of 20 nm sized $In_{0.5}Ga_{0.5}As$ QDs are differently separated. It indicates that the side-to-side neighboring QDs can grow almost independently. With our minimum achievable lateral size, 20 nm, the controllable inter-dot distance can be down to 25 nm, meaning QDs nearly touching their neighbors. Detailed studies show that the lateral size

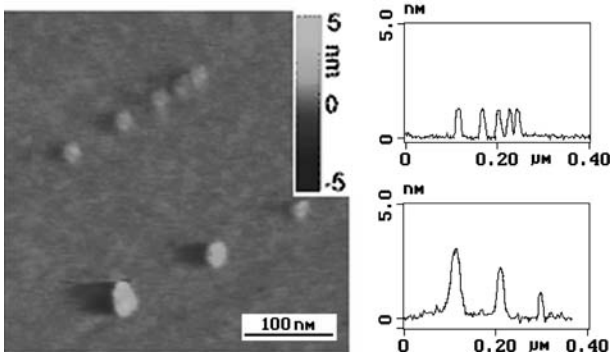


**Fig. 3** AFM image and cross-section profiles for growing 3.5 ML of $In_{0.5}Ga_{0.5}As$ on a GaAs surface patterned with differently distant (upper half) and differently sized (lower half) holes fabricated by AFM oxidation and oxide removal

is determined by the hole diameter without changing with coverage, whereas the QD height increases with coverage at a speed related to the hole size [15]. The lower half of Fig. 3 shows three different QDs which were formed on three different holes about 50, 30 and 20 nm large. After depositing 3.5 ML of $In_{0.5}Ga_{0.5}As$, the on-site QDs exhibit the same lateral sizes as the original holes but different heights of 3, 2, and 1 nm.

The minimum available interdot distance of less than 30 nm enables observable coherent lateral interaction between neighboring QDs [20, 21]. The simultaneous availability of various QD sizes provides a way to controllably construct asymmetric QD molecules. These open the way to apply the present technique in quantum computation using site-controlled semiconductor QDs [22]. In a proposed model of quantum computer [23], one qubit consists of a big QD as the main dot and a few small QDs as the operation dots, as is schematically illustrated in Fig. 4a. The inter-qubit interaction is controlled by pushing an electron into the main dots (weakly or not coupled) or neighboring operation dots (strongly coupled). In the stand-by state, the electron with spin up or down stays in the main dot. Applying a suitable $\pi$-pulse to any qubit, the electron will transfer to an operation dot. The quantum gate operation is implemented via swapping between the electron spins in operation dots belonging to neighboring qubits. Figure 4b shows such a QDs structure fabricated by the present technique. The big and small dots are ~30 and ~20 nm in diameter and the center-center distance between big and small sites is 40 nm. The height of oxide dots are about 1.5 (big) and 1.2 nm (small) and the depth of holes are 1.4 (big) and 1.1 nm (small),

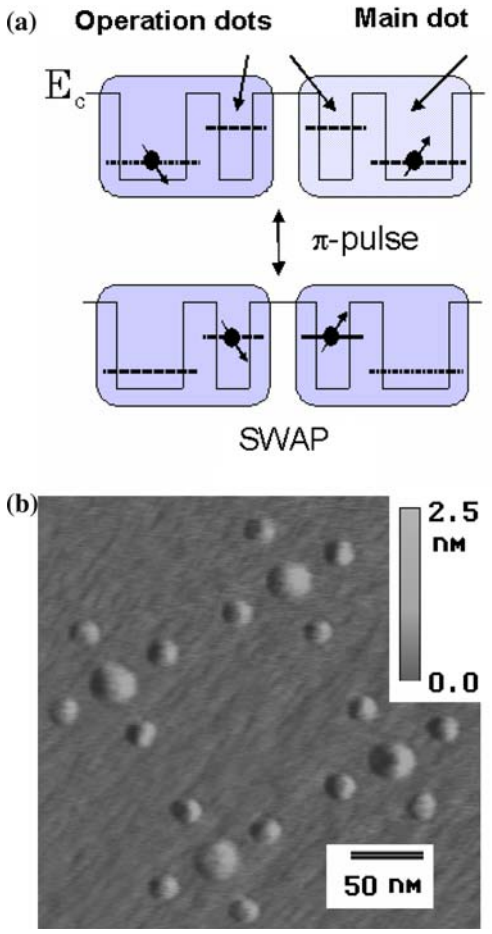


**Fig. 4** (**a**) Qubit structure and operation of an all-optical quantum computer using electron spins in asymmetrically coupled QDs; (**b**) AFM image of qubit-structured QDs array, which fits the model in (**a**), fabricated using the present technique

which are as expected. Of course, to better satisfy the requirement of qubit construction, more precise control should be realized. For instance, control scale of 10 nm can be available if a recently developed carbon-nanotube AFM tip is readily adopted in AFM lithography on semiconductor surface.

## Optical characteristics

For the application of site-controlled QDs, their optical properties were characterized. Here we are going to show an example of InAs/InP QDs [16], which are the candidate of single photon emitters at telecommunication bands of silica-based optical fibers, *i.e.* from 1.3 to 1.55 μm [24, 25]. The sample preparation was performed on the surface of a flat semi-insulating InP(001) substrate using the present technique. After formation of holes by chemical etching, MOCVD was carried out to form InAs QDs at the holes sites. In this case, the initial native oxides are removed by the reactive atomic hydrogen generated from decomposed $PH_3$. The InAs QDs, formed with 1.4 ML of InAs coverage, are 500 nm separated for the purpose of single dot photoluminescence (PL) measurements, as shown in Fig. 5a. The cross section of such QDs is depicted schematically by the upper half in Fig. 5b, where it is shown that they have a deep part, in fact ~2 nm, below the wetting layer. Formation of site-controlled QDs are immediately followed by a so-called ''double-cap'' growth [26–29]. The first cap process cuts the outstanding part of QDs beyond the surface, as shown by the lower diagram of Fig. 5b. As a result, the first cap layer thickness determines the final height of QDs.

The micro-PL was measured with the 532 nm line of a Nd:YAG laser on samples with the first cap layer thickness varying from 0.3 to 2 nm. At an arbitrary position, we first observe the strong wetting layer emission around 985 nm as shown in the inset of Fig. 6. In the region of site-controlled QDs, narrow PL peaks are observed. Taking the detector efficiency into account, the luminescence intensity is comparable to that of InAlAs/AlGaAs QDs conventionally self-assembled in S–K mode [30]. The site-dependence of micro-PL following the controlled sites of QDs confirms that these single peaks come from the site-controlled single InAs/InP QDs [16]. A typical single dot PL spectrum for each sample is presented in Fig. 6. For the sample with the first cap of 2 nm, the QDs emissions are estimated to be centered around 1.7 μm, which is beyond the instrument limit. As a result, most of the QDs are undetectable but few dots emitting at shorter wavelengths are observed, as exemplified by a peak at 1.59 μm in Fig. 6. The other three peaks in Fig. 6, at 1.33, 1.42 and 1.47 μm reflect approximately the average emission wavelength over all dots in one sample. The change of average position

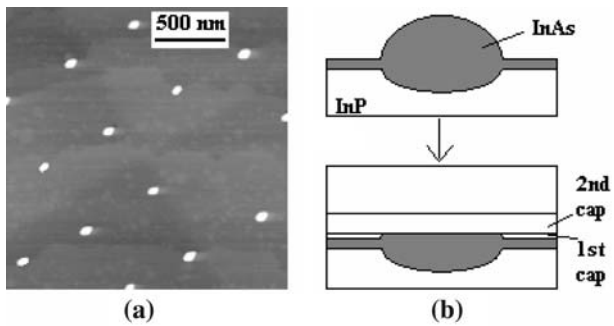


**Fig. 5** (**a**) AFM image of site-controlled InAs/InP QDs after MOCVD regrowth of 1.4-ML InAs; (**b**) the schematic demonstration of the following ''double-cap'' growth

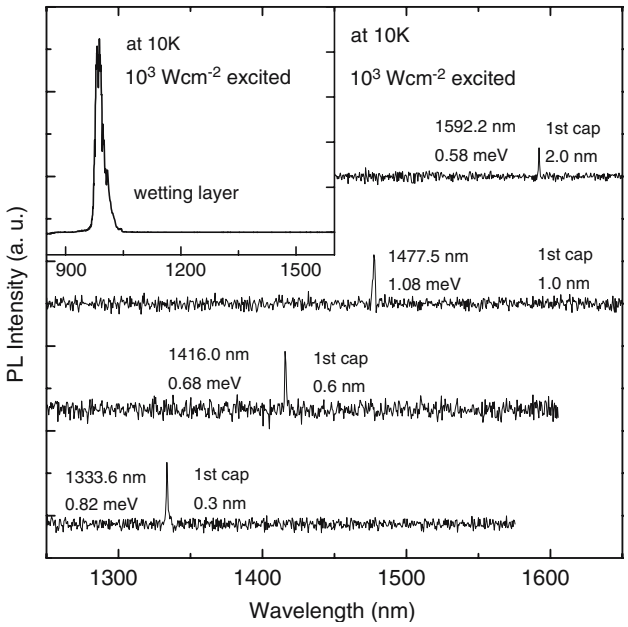


**Fig. 6** Typical single dot micro-PL peaks from site-controlled InAs/InP QDs with different thickness of the first cap layer. The inset shows the PL of the wetting layer

follows the quantum confinement effect and indicates that the emission wavelength can be tuned by the fabrication conditions to fit the application requirements. The site-controllability of single dot emitters at telecommunication bands is thus revealed.

The single dot peaks look broader than conventionally grown self-assembled quantum dots, about 0.8 meV in full width at half maximum, but they are the same as that of InAs/InP QDs produced at nanotemplates [12], in which the formed QDs are a few hundred nm far away from the initially patterned surface processed by electron beam lithography. This suggests that regrowth of QDs directly on a chemically processed substrate may not be a severe factor to degrade the dot quality in our technique.

However, the possibly imperfect interface between the chemically processed substrate and the overgrown QDs might play some role in the optical behaviors of site-controlled QDs. This is implied by the excitation density dependence of the single dot micro-PL intensity. It is found that the integrated intensities of single dot micro-PL peaks do not exhibit a universal excitation density dependence but vary from linear to quadratic for different QDs. Three examples, for dots a, b and c from the sample with first cap of 0.3 nm, shown in Fig. 7a by solid symbols follow the power law function with index of 1.0, 1.32 and 2.0, respectively. We may refer to a model in terms of nonradiative process as in quantum wells [31], in which the excitation density $I_{ex}$ satisfies:

$$\alpha I_{ex} = \frac{n}{\tau_n} + Bnp = \frac{p}{\tau_p} + Bnp \quad (2)$$

where n(p) is the electron (hole) number in the QD, $\tau_n(\tau_p)$ is the nonradiative decay time of electrons (holes), $B$ is the radiative recombination rate and $\alpha$ is an coefficient associated with the absorption. Here the radiative recombination takes the form of $B$np because the electrons and holes can be captured independently in a single QD [32]. Denoting PL intensity as $L$=$B$np=np/$\tau_0$ with $\tau_0$ the rediative lifetime, and defining $(\tau_n\tau_p)^{1/2} = \tau$ as the normalized nonradiative lifetime, Eq. (2) can be reduced to:

$$\alpha I_{ex} = L + \sqrt{L\tau_0}/\tau. \quad (3)$$

It is easy to see that $L \approx \alpha^2\tau^2 I_{ex}^2/\tau_0$ when $\tau^2/\tau_0$ is sufficiently small, and $L \approx \alpha\ I_{ex}$ while $\tau^2/\tau_0$ is sufficiently large. Providing the nonradiative lifetime $\tau$ varies from dot to dot, the different excitation density dependence of PL intensity can be understood. In Fig. 7a, it is clear that the results at 10 K are well fitted by Eq. (3) with different $\tau$ for different peaks. The dot dependent

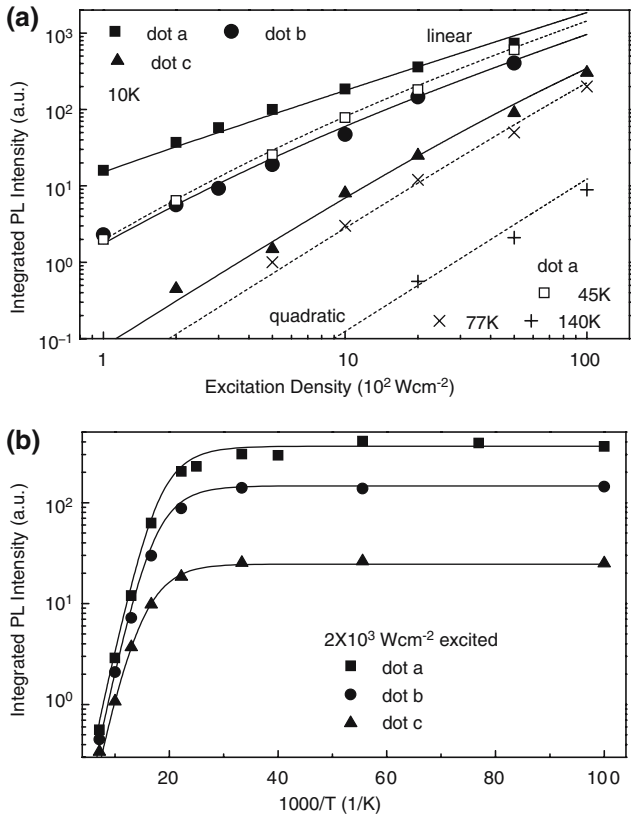


**Fig. 7** (**a**) Excitation density and (**b**) temperature dependences of the single dot PL intensities of site-controlled InAs/InP QDs. Lines show the fitted results using Eqs. (3) and (4)

nonradiative lifetime is thought to be the result of different number of nonradiative centers in different dots. Considering the chemical processing before QD regrowth, the nonradiative centers might be some impurities or defects in the vicinity of QDs, which are survived from the incomplete surface cleaning.

The effects of impurities/defects can be further suggested by the temperature dependence of the single dot emission. The symbols other than solid ones in Fig. 7a show the excitation density dependence at elevated temperatures for dot a. It is seen that increasing temperature leads to more and more quadratic excitation density dependence of PL intensity. These can also be well fitted by Eq. (3) but with $\tau$ more and more shortened with increasing temperature. In detail, Fig. 7b demonstrates that, at a fixed excitation density, the PL intensity of each dot is nearly constant at low temperatures but thermally quenched at higher temperatures. These data are suggestive of an expression of the nonradiative lifetime $\tau$ as:

$$\tau^{-1} = \tau_1^{-1} + \tau_2^{-1} e^{-E/kT}, \quad (4)$$

where $\tau_1$ and $\tau_2$ are time constants, $E$ is an activation energy, $k$ is the Boltzmann constant and $T$ is the temperature. The solid lines in Fig. 7b indicate that the experimental results are well fitted to Eq. (3) together with (4). What is more important, all the site-controlled QDs show an activation energy $E \approx 22.5$ meV, suggestive of phonon scattering as in conventionally self-assembled QDs [33] at higher temperatures. In addition, $\tau_1$ is dot dependent and close to the value of $\tau$ at 10 K, while $\alpha$, $\tau_0$ and $E$ are almost dot independent. The parameter $\tau_2$ is also dot dependent with the same trend as but more weakly than $\tau_1$. This may be ascribed to impurities/defects enhanced photon scattering [34], as a result of imperfect interface between site-controlled QDs and their substrate.

Nevertheless, the PL from the wetting layer is as normal, *i.e.* it does not show a complicated excitation density dependence but simply a linear behavior in a lower excitation range (not shown). It means that the nonradiative process due to interface impurities/defects does not have an obvious effect in the wetting layer. Therefore, the impurities/defects exist mainly at QD sites. This is because there are high density of steps with dangling bonds at the hole sites. It may be concluded that these impurities/defects are not intrinsic in our present technique. They will be well suppressed in the future by improving the fabrication technique, e.g. using in situ atomic hydrogen irradiation to remove oxide dots, optimizing the annealing condition and finely controlling the AFM oxidation.

Although our site-controlled QDs are open to be improved, the present quality is not below the limit of application in quantum communication because conventionally self-assembled InAlAs/AlGaAs QDs of similar quality have exhibited single photon emission [35]. We are currently struggling to perform single photon transmission using such site-controlled QDs as the source working at telecommunication bands for silica-based optical fibers.

## Summary

We developed an AFM-assisted technique to control the position and size of self-assembled semiconductor QDs. The site precision of QDs is as good as ± 1.5 nm and the QD size fluctuation can be within ± 5%, which is better than that in conventional S–K growth. The controllable minimum lateral size of 20 nm, the interdot distance as small as the diameter of QDs and the simultaneous control of differently sized QDs enable constructing QD qubits to be applied in quantum computing. The optical quality of such site-controlled QDs is found comparable to conventionally self-assembled InAlAs/AlGaAs QDs. The InAs/InP QDs fabricated by this technique are shown to be a candidate of site-controlled single-photon emitters working at telecommunication bands for the application in quantum communication. What is to be improved may be the imperfection of the interface between QDs and the processed substrate, where impurities/defects influence the optical quality of site-controlled QDs.

## References

1. D. Bimberg, M. Grundmann, N.N. Ledentsov, *Quantum Dot Heterostructures* (Widley, New York, 1999)
2. H. Sakaki, Jpn. J. Appl. Phys. **28**, L314 (1989)
3. T. Takagahara, Surf. Sci. **267**, 310 (1992)
4. H.Z. Song, K. Akahane, S. Lan, H.Z. Xu, Y. Okada, M. Kawabe, Phys. Rev. B **64**, 085303 (2001)
5. N.H. Bonadeo, J. Erland, D. Gammon, D. Park, D.S. Katzer, D.G. Steel, Science **282**, 1473 (1998)
6. L. Besombes, J.J. Baumberg, J. Motohisa, Phys. Rev. Lett. **90**, 257402 (2003)
7. C. Santori, D. Fattal, J. Vučković, G.S. Solomon, Y. Yamamoto, Nature **419**, 594 (2002)
8. Z. Yuan, B.E. Kardynal, R.M. Stevenson, A.J. Shields, C.J. Lobo, K. Cooper, N.S. Beattie, D.A. Ritchie, M. Pepper, Science **295**, 102 (2002)
9. D. Loss, D.P. DiVincenzo, Phys. Rev. A **57**, 120 (1998)
10. T. Ishikawa, T. Nishimura, S. Kohmoto, K. Asakawa, Appl. Phys. Lett. **76**, 167 (2000)

11. H. Lee, J.A. Johnson, M.Y. He, J.S. Speck, P.M. Petroff, Appl. Phys. Lett. **78**, 105 (2001)
12. D. Chithrani, R.L. Williams, J. Lefebvre, P.J. Poole, G.C. Aers, Appl. Phys. Lett. **84**, 978 (2004)
13. H.Z. Song, T. Ohshima, Y. Okada, K. Akahane, T. Miyazawa, M. Kawabe, N. Yokoyama in *Proceedings of the 26th ICPS*, Edinburgh, 29 July- 2 August 2002, P.32
14. U.F. Keyser, H.W. Schumacher, U. Zeitler, R.J. Haug, K. Zberl, Appl. Phys. Lett. **76**, 457 (2000)
15. H.Z. Song, Y. Nakata, Y. Okada, T. Miyazawa, T. Ohshima, M. Takatsu, M. Kawabe, N. Yokoyama, Phys. E **21**, 625 (2004)
16. H.Z. Song, T. Usuki, S. Hirose, K. Takemoto, Y. Nakata, N. Yokoyama, Y. Sakuma, Appl. Phys. Lett. **86**, 113118 (2005)
17. A. Hirai, K.M. Itoh, Physica E **23**, 248 (2004)
18. Y. Okada, Y. Iuchi, M. Kawabe, J.S. Harris, Jr., J. Appl. Phys. **88**, 1136 (2000)
19. Zh. M. Wang, Y.I. Mazur, Sh. Seydmohamadi, G.J. Salamo, H. Kissel, Appl. Phys. Lett. **87**, 213105 (2005)
20. H.Z. Song, S. Lan, K. Akahane, K.Y. Jang, Y. Okada, M. Kawabe, Solid State Communications **115**, 195 (2000)
21. D.L. Huffaker and D.G. Deppe, Appl. Phys. Lett. **73**, 366 (1998)
22. T. Ohshima, H.Z. Song, Y. Okada, K. Akahane, T. Miyazawa, M. Kawabe, N. Yokoyama, Phys. Stat. Sol. (c) **4**, 1364 (2003)
23. T. Ohshima, Phy. Rev. A **62**, 062316 (2000)
24. K. Takemoto, Y. Sakuma, S. Hirose, T. Usuki, N. Yokoyama, Jpn. J. Appl. Phys. (part B) **43**, L349 (2004)
25. K. Takemoto, Y. Sakuma, S. Hirose, T. Usuki, N. Yokoyama, T. Miyazawa, M. Takatsu, Y. Arakawa, Jpn J. Appl. Phys. (part B) **43**, L993 (2004)
26. C. Panranthoen, N. Bertru, O. Dehaese, A. LeCorre, S. Loualiche, B. Lambert, G. Patriarche, Appl. Phys. Lett. **78**, 1751 (2001)
27. S. Raymond, S. Studenikin, S.J. Cheng, M. Pioro-Ladrière, M. Ciorga, P.J. Poole, M.D. Robertson, Semicond. Sci. Technol. **18**, 385 (2003)
28. Y. Sakuma, K. Takemoto, S. Hirose, T. Usuki, N. Yokoyama, Physica E **26**, 81 (2005)
29. Y. Sakuma, M. Takeguchi, K. Takemoto, S. Hirose, T. Usuki, N. Yokoyama, J. Vac. Sci. Technol. B **23**, 1741 (2005)
30. T. Yokoi, S. Adachi, H. Sasakura, S. Muto, H.Z. Song, T. Usuki, S. Hirose, Phys. Rev. B **71**, 041307R (2005)
31. W. Feng, Y. Wang, J. Wang, W.K. Ge, Q. Huang, J.M. Zhou, Appl. Phys. Lett. **72**, 1463 (1998)
32. K.F. Karlsson, E.S. Moskalenko, P.O. Holtz, B. Monemar, W.V. Schoenfled, J.M. Garcia, P.M. Petroff, Appl. Phys. Lett. **78**, 2952 (2001)
33. V.I. Ignatiev, E.I. Kozin, S.V. Nair, H.W. Ren, S. Sugou, Y. Masumoto, Phys. Rev. B **61**, 15633 (2000)
34. M. Pepper, J. Phys. C **13**, L709 (1980)
35. S. Kimura, H. Kumano, M. Endo, I. Suemune, T. Yokoi, H. Sasakura, S. Adachi, S. Muto, H.Z. Song, S. Hirose, T. Usuki, Jpn. J. Appl. Phys. **44**, L793 (2005)